Journal of Materials Science and Chemical Engineering, 2026, 14(3), 63-87
https://www.scirp.org/journal/msce
ISSN Online: 2327-6053
ISSN Print: 2327-6045

Steady-State and First-Order Transient Thermal Performance of an Axially Finned Heat Pipe Heat Exchanger—AFHPHE in the Evaporator Region

Élcio Nogueira

Department of Mechanical and Energy (DME), Faculty of Technology (FAT), State University of Rio de Janeiro (UERJ), Resende, Brazil
Email: elcio.nogueira@uerj.br

How to cite this paper: Nogueira, É. (2026) Steady-State and First-Order Transient Thermal Performance of an Axially Finned Heat Pipe Heat Exchanger—AFHPHE in the Evaporator Region. *Journal of Materials Science and Chemical Engineering*, **14**, 63-87.
https://doi.org/10.4236/msce.2026.143006

Received: January 30, 2026
Accepted: March 15, 2026
Published: March 18, 2026

Abstract

This article presents a refined analysis of evaporator region of an axially finned heat pipe heat exchanger (AFHPHE), which is being theoretically evaluated for use in operating room air conditioning systems. The analysis provides an unusually simple first-order transient model for a multi-thermosiphon bundle heat exchanger. The objective is to provide an approximate theoretical prediction of the first-order transient response of a heat exchanger with 49 closed two-phase thermosiphons, with 30 axial fins in each thermosiphon, in the evaporator region. The steady-state solution for the heat exchanger is already well established, with theoretical experimental comparisons performed with other similar heat pipe systems presented in the literature. The transient solution uses steady-state results of the working fluid and the heat exchanger to validate the conclusions. The working fluid is the refrigerant R404a, widely used in similar systems. The transient results presented are the temporal variations in the heat exchange rate, working fluid temperatures, heat pipe wall temperatures, and air outlet temperatures. Variations in the working fluid filling rates are simulated to demonstrate the consistency of the developed model. Although the theoretical model appears logically consistent, its irrefutable validation depends on future experimental results, which represents a significant challenge.

Keywords

Heat Exchangers, Two-Phase Closed Thermosyphons, Transient Regime, Computational Modelling, Refrigerant R404a

1. Introduction

The main objective of this work is to provide an approximate transient analytical solution for the thermal characteristics of a heat exchanger with 49 finned axial thermosiphons, using consolidated steady-state solution results. The system under analysis is schematically represented below, Figure 1(a) and Figure 1(b), as an initial proposal for the implementation of the heat exchanger.

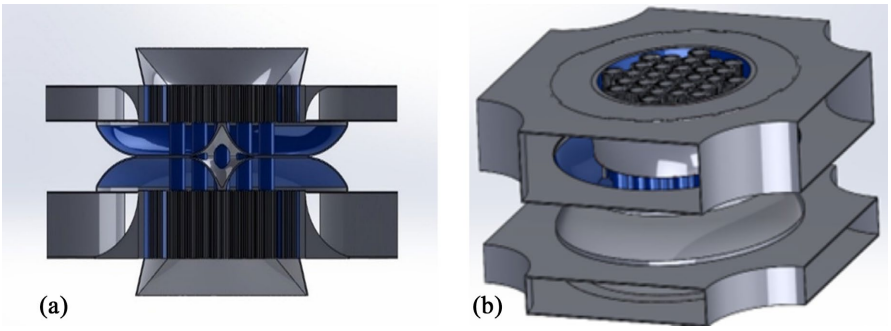

Figure 1. Initial design of a heat exchanger with axially finned heat pipes.

The analysis presented involves three main stages, focusing on the evaporator region of the heat exchanger. The first analyzes the working fluid, in relation to pressure and temperature, as a function of the filling rate. Next, a steady-state analysis of the evaporator is presented, obtaining the thermal quantities of interest for validating the following stage, which involves the variations of the thermal quantities over time at the beginning of the heat exchanger's operation.

Before presenting the analyses mentioned above, it is necessary to discuss details of some previously published works in the literature, which served as the basis for what is presented in this article.

Hichem Farsi *et al.* [1] present experimental and theoretical results for a two-phase closed thermosiphon in transient regime. They develop a mathematical model to obtain an analytical expression for the response time of the system under analysis. They conclude that the presented model is a simple and efficient tool for both transient and steady-state regimes. The theoretical analysis focuses on two main aspects of the system: the evaporator wall and the working fluid, showing good agreement with experimental results.

J. Kirk Storey [2] used a numerical model to represent the transient operation of a thermosiphon. The model includes transient conduction in the vessel wall and shear stress between the ascending vapor and the descending film in the thermosiphon. The difference in the developed model reports to temporal changes in the effective length of the vapor space due to the expansion and contraction of non-condensable gases. The model assumes a quasi-steady one-dimensional vapor flow, a transient one-dimensional flow in the descending liquid film, and transient behavior in the liquid pool in the evaporator. The model assumes transient two-dimensional conduction in the thermosiphon wall. The governing equations were developed and written in finite difference form. An experiment was con-

ducted to validate the numerical model. The uncertainty obtained is on the order of 2.3%.

Fernando H. Milanez and Marcia H. Mantelli [3] developed an analytical model to analyze the thermal performance of a rectangular enclosure heated by two-phase thermosiphons. They predicted the temperatures and thermal resistances between the enclosure elements based on experimental data. The differences between the model and the experimental data range from 3.4˚C to 7.6˚C. They concluded that the thermal resistances of the joints are difficult to predict and use the model to estimate the relative importance of the three modes of heat transfer within the enclosure. The results obtained demonstrate that the isothermal characteristic does not lead to effective natural convection heat transfer. They show that the usual approach of riveted joints is thermally inefficient.

R. Parand *et al.* [4] present a theoretical investigation of the transient behavior of a thermosiphon. It uses a lumped transient model to simulate the heat pipe's response time. MATLAB is used to develop the lumped analysis model to estimate the thermosiphon temperature, and the model is implemented using Simulink. The paper states that the model can be used as a simple tool for modeling and designing transient heat pipes, and that the results show general agreement with numerical models available in the open literature.

Karima Esmail Amori and Muhanad Latif Abdullah [5] experimentally and theoretically investigated the thermal characteristics of a closed two-phase heat pipe. They fabricated a closed two-phase heat pipe, using Fluorocarbon FC-72 (C6F14) as the working fluid, to examine the effect of inlet heat flux in the range of 250 - 1253 W/m^2. They also analyzed a 70% fill rate under various tilt angles. They experimentally monitored the temperature distribution along the heat pipe, the inlet heat in the evaporator section, and the outlet heat from the condenser. A mathematical model was developed to investigate the steady-state heat transfer performance. An analytical steady-state model is presented to determine important parameters in the design of a closed two-phase heat pipe. Parameters analyzed through the theoretical model include temperature levels and heat transfer coefficients. Experimental and simulation results from this work showed good agreement.

Davoud Jafari *et al.* [6] present experimental results and numerical simulation of a two-phase closed thermosyphon (TPCT) in transient regime. The developed model performs heat transfer analysis in the tube wall, vapor core, condensate liquid film region, and pool region, aiming to maximize heat pipe performance and analyze the possibility of Dryout and geyser boiling phenomena occurring in the evaporator. In summary, they report that theoretical and experimental results align well, demonstrating that the two-dimensional model effectively predicts system behavior in transient and critical conditions such as Dryout.

Zhongchao Zhao *et al.* [7] study the transient thermal performance of phase change and heat and mass transfer in a closed two-phase thermosyphon using computational fluid dynamics (CFD). Deionized water is used as the working

fluid. The CFD model reproduces evaporation and condensation in the thermosiphon at different heating inlets. Variations in average wall temperatures indicate that this thermosiphon reaches a steady state after 19 s.

Igor Cavalcante da Silveira [8] clarifies that heat pipes are devices capable of transporting high rates of thermal energy over long distances, although there are still few applications using heat pipes in Brazil. In this sense, he constructs an experimental system for analyzing the thermal performance of a thermosyphon subjected to a heat flux of 1000 W/m^2. Furthermore, he develops two mathematical models to estimate the operating temperature of the experimental system. The lumped analysis model is based on energy balance and the effectiveness method (ε-NUT) for heat exchangers. The steady-state solution model uses the heat diffusion equation and employs the Generalized Integral Transform Technique (GITT). Comparisons between theoretical and experimental models generally show satisfactory results, and the experimentally obtained temperature profiles allow for the definition of appropriate correlations for thermosiphon operation.

Élcio Nogueira [9] develops a theoretical model using the thermal efficiency method to improve energy-saving in air conditioning systems. The model uses a method localized to an individually finned heat pipe heat exchanger (IFHPHE) and obtains results for overall thermal performance analysis. Comparisons with experimental results show excellent agreement, demonstrating that the theoretical approach is consistent and can be used for the analysis of heat exchangers that utilize heat pipes.

Hao Liu *et al.* [10] perform for the first time field tests of a flexible thermosiphon for geothermal using a super-long flexible thermosiphon made of corrugated tubing with a total length of up to 32 m. The developed equipment was field-tested during drilling to evaluate its potential use in shallow geothermal exploration. They investigate the seasonal dependence of local groundwater temperature and air temperature, the corresponding thermal response, and its heat transfer characteristics. They analyze the groundwater temperature recovery characteristics during unidirectional heat extraction operation through a combination of field tests and CFD simulation. They demonstrate that the analyzed device can operate effectively, since the vaporization of the working fluid occurs throughout the evaporator. They clarify that the use of corrugated tubing prevents the formation of a very high liquid layer in the evaporator. They conclude that steady-state analysis reveals that groundwater temperature plays the most important role in thermal performance, followed by flow rate and cooling water temperature. They recommend that the heat extraction rate be kept below 30 W/m^2 at the drilling site, to ensure good sustainability.

Daniel J. Brough [11] states that high-pressure water-heat exchangers (HPHEs) can be effectively installed where traditional heat exchangers fail, and the heat flow is considered "unrecoverable". Heat recovery using HPHEs can increase energy efficiency, decrease fuel consumption, and reduce emissions. The performance of HPHEs depends on steady-state or average input values, and as such, it is im-

portant to determine the transient performance of a heat exchanger. The simulation methodology assists in visualizing transient energy recovery, aids the design process, and provides greater confidence in the expected performance before HPHE installation. Experimental validation ensures that the methodology can be used in simulations of complete HPHE systems.

Wenwen Zhang *et al.* [12] developed a two-phase model where a set of six equations describes the two-phase flow, encompassing mass equations, momentum equations, and energy equations. To obtain numerical solutions of the partial differential equations, in a stepped mesh structure, they employed the second-order Lax-Wendroff scheme in a discrete linear system, complemented by the inclusion of a flow limiter. Small-scale TPLT tests were used to evaluate the accuracy and reliability of the numerical method. Simulations were performed under two conditions: filling rates of 45% and 64%. The model results show good agreement with experimental data and provide information about the complex two-phase flow that cannot be obtained through experiments.

Guo Li *et al.* [13] present a transient thermosiphon model to meet thermal protection requirements. The objective is to build a simulation tool to capture the transient characteristics of the thermosiphon. The results obtained demonstrate good agreement with experimental results, remaining within a 10% error range. The study investigated steady-state and transient initialization processes with various heat fluxes and filling rates and confirmed that a low filling rate can result in a serious overheating problem in the upper region of the evaporation section.

Élcio Nogueira *et al.* [14] compare two heat exchangers that use finned heat pipes, using refrigerant R404a. One uses radial fins in crossflow and the other uses axial fins in parallel flow. The analysis uses the Thermal Efficiency Method to analyze thermal irreversibilities and the second Law of Thermodynamics to analyze viscous irreversibilities, using the Bejan number. They demonstrate that the axially finned heat pipe heat exchanger (AFHPHE) has potential for use in air conditioning systems operating in surgical rooms and other systems.

Élcio Nogueira [15] publishes a book presenting applications of theories related to heat exchangers. The theories developed relate to thermal irreversibilities and viscous irreversibilities. It is a theory that encompasses the concepts usually applied in heat exchangers but breaks new ground by introducing the idea of Thermal Efficiency. A new path with consolidated foundations and applicable to all types of heat exchangers.

Wandong Bai *et al.* [16] state that closed two-phase thermosiphon (TPCT) has great potential in solar thermal collectors, although research on this topic is limited. This study investigates the effects of condensation cooling, heating power, and working fluid filling rate on the heat transfer characteristics of TPCT. They develop a model based on the Lee equation, using Nusselt theory and the principle of thermal balance. The results obtained indicate that the two-phase flow exhibits intermittent boiling, continuous boiling, and annular flow modes under different operating conditions. The two-phase flow patterns determine the temperature be-

havior and overall heat transfer performance. This work contributes to the understanding of the mechanisms governing heat transfer, providing guidance for controlling operating conditions in its application.

Fernando da Silva Almeida *et al.* [17] report that there has been a notable interest in new heat transfer technologies for building envelopes and that heat pipes and thermosiphons deserve special attention among the technologies employed. The study provides valuable information on the main applications, numerical modeling approaches, performance parameters, and thermo-energetic applications. They state that the use of heat pipes and thermosiphons is promising for improving thermal comfort in buildings. They note that there is a gap in the study of these technologies, and that studies focus on applications in walls that take advantage of solar radiation. They state that there are gaps in the incorporation of these technologies into building envelopes, such as internal partitions, floors, ceilings, and shading elements, and that numerical modeling lacks validation through real-world applications, and that full-scale studies are also scarce. They note the need for research on alternative geometries for heat pipes to improve their adaptability to buildings, as well as on lower-cost and environmentally friendly commercial refrigerants.

Mohammad Khalili *et al.* [18] state that effective heat dissipation is crucial in various thermal management applications in electronic systems, renewable energy, and heating and cooling systems. Closed two-phase thermosiphons have been widely adopted in these fields. They present a design for a TPCT that incorporates a unique inner tube, cone-shaped in the evaporator. The innovation aims to minimize vapor-liquid interaction within the main tube, enhancing greater heat transfer efficiency. The proposed device is evaluated using water and ethanol as working fluids. Results indicate that the ideal filling rate depends on the working fluid. Water shows the best performance with filling rates of 55% and 85%, while ethanol reaches its optimum at 70%. They demonstrate that increasing the heat input reduces thermal resistance but also raises the operating temperatures of the TPCTs under analysis. The TPCT incorporating an inner tube demonstrates a significant improvement in thermal performance when using ethanol as the working fluid.

2. Methodology

2.1. Analysis of the Work Fluid

The numerical procedure used in this first stage of the work is presented below.

Considering that the saturation temperature is strictly valid at the liquid-vapor interface, the approximate value of the axial pressure is obtained along the evaporator. From this information, the local temperature values are obtained using a pressure-temperature table for R404a.

$$P_f\left(L_f\right) = P_{sat} + \rho_l * g * \left(L'_{Ev} - L_f\right) \tag{1}$$

$$L'_{Ev} = FR * L_{Ev} \quad \text{with } L_{Ev} = 220 \text{ mm} \tag{2}$$

$$\Delta H \le L_f \le L'_{Ev};\ \Delta H = 10^{-3} \tag{3}$$

$P_f\left(L_f\right)$ is associated with the pressure variation in the axial direction in the evaporator; L_f with the fluid height in the evaporator; P_{sat} is the saturation temperature of the fluid at the liquid-vapor contact interface; ρ_l is the specific mass of the liquid at the local pressure; $L'_{Ev} \le L_{Ev}$ is the length of the liquid portion in the evaporator; FR is the filling rate defined a priori ($50\% \le FR \le 100\%$). The values below are associated with refrigerant R404a.

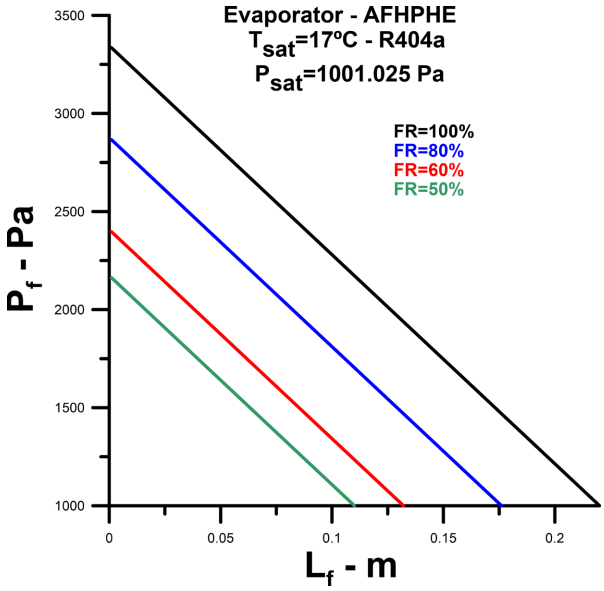

Figure 2. Working fluid pressure in axial direction as a function of the filling rate.

Figure 2 represents the pressure variation along the axial direction in the evaporator occupied by the working fluid, as a function of the filling rate. The pressure is maximum at the lower position of the thermosiphon and decreases as it approaches the liquid-vapor interface. The local pressure depends on the filling rate, since the interface position is the reference for obtaining the local pressure. When the filling rate is equal to 100%, the lowest pressure, P_{sat}, is found at the maximum axial position for the evaporator under analysis (220 mm). The same occurs for lower filling rates, with the maximum position varying in the axial direction ($L'_{Ev} < 220$ mm).

Figure 3 shows the variation of pressure as a function of temperature for R404a. The local temperature of the fluid increases with increasing pressure, with the saturation temperature having the lowest value, equal to 17˚C.

The equation that represents the variation of the fluid temperature in relation to P_f as shown in Figure 3, is represented by Equation (4) below.

$$T_f = -21.98107593 + 0.04480121903 * P_f - 5.93743432210^{-6} * P_f^2 \tag{4}$$

T_f represented by Figure 4, is the local temperature of the working fluid in the evaporator, associated with P_f. The working fluid temperature is equal to the saturation temperature at the maximum position occupied by the fluid, which is

dependent on the filling rate. The first approximate average values for the working fluid temperature (arithmetic mean), as a function of the filling rate, are highlighted.

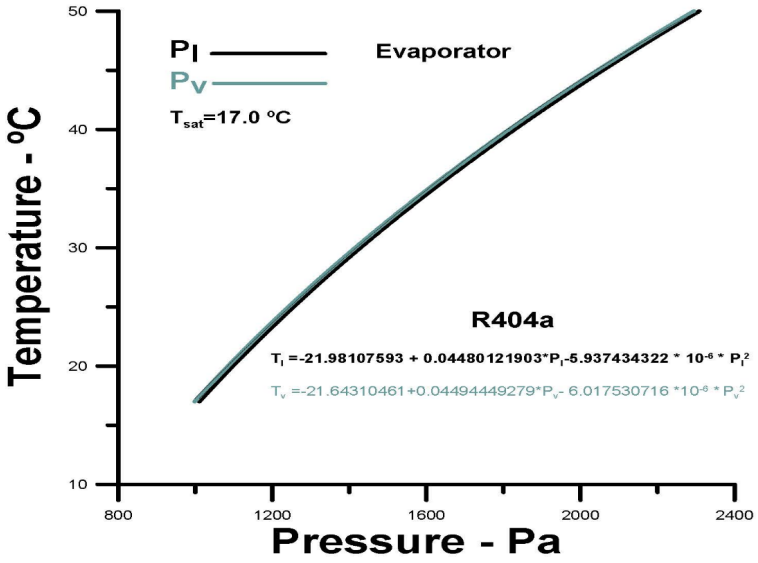

Figure 3. Temperature versus pressure (Thermodynamic Tables R404a).

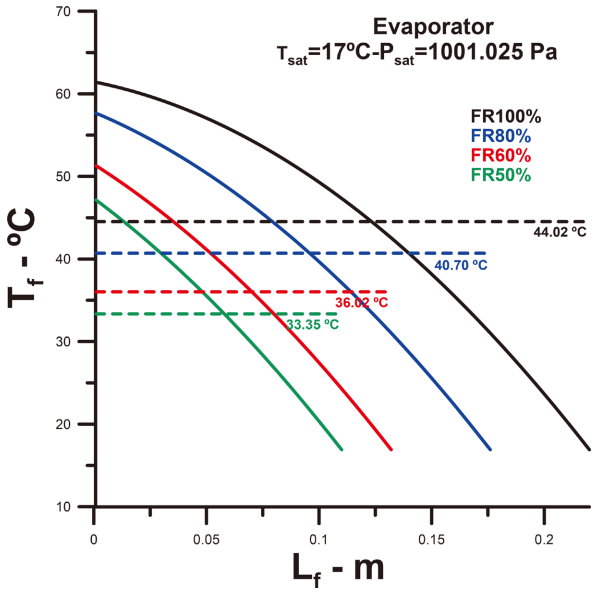

Figure 4. Working fluid local temperature in axial direction as a function of the filling rate.

2.2. Steady State Analysis—Formulation for Evaporator

The solution method is analytical. Initially, the Thermal Efficiency Method was used to obtain steady-state thermal results in the evaporator of the heat exchanger. Using the local values obtained, the average temperature along the length of the evaporator can be approximately determined, considering the filling rate. These average values obtained were considered the average temperature of the evaporator in steady state. The procedure for obtaining average values for other quantities

of interest is the same as that used to obtain average temperature. Average values are obtained through a numerical procedure called the trapezoidal rule, which is slightly more precise than the arithmetic mean mentioned above.

The formulation presented for the evaporator of the AFHPHE in steady state conditions is like that presented by Élcio *et al.* [14].

Equations (5)-(44) represent the operation of the evaporator in steady state, under conditions of air inlet temperatures in the heat exchanger.

The saturation temperatures of the working fluid and inlets:

$$T_{sat} = 17.0^{\circ}\text{C};\ T_{Evin} = 30.0^{\circ}\text{C}\ \text{ or }\ T_{Evin} = 25.0^{\circ}\text{C} \tag{5}$$

The mass flow rates in the evaporator:

$$\dot{m}_{air} = 0.20\ \text{kg/s default} \tag{6}$$

The number of heat pipes and the number of fins per heat pipe are defined by the expressions below.

$$N_{HP} = 49\ \text{default} \tag{7}$$

where, by AFHPHE:

$$N_R = \sqrt{N_{HPb}},\ \ N_{HPb} = 16\ \text{heat pipes} \tag{8}$$

$$N_{HPR} = N_R + \left(N_R + 1.0\right) \tag{9}$$

N_{HPR} is the number of heat pipes per row.

Finally, the number of heat pipes is represented by equation (10).

$$N_{HP} = N_{HPR} * \left(N_R + 1.0\right) + N_R \tag{10}$$

The radial configuration with 49 tubes is represented in **Figure 5** below. The analysis, developed for application to heat exchangers, showed that the thermosiphons were arranged in a radially homogeneous and absolute manner. The homogeneous distribution of the tubes allows the average air velocity at a given axial position, from the air inlet, to be the same in all tube sections, considering that the air passage areas and heat exchange areas have the same configurations. These conditions, when imposed, facilitate analysis along the heat exchanger.

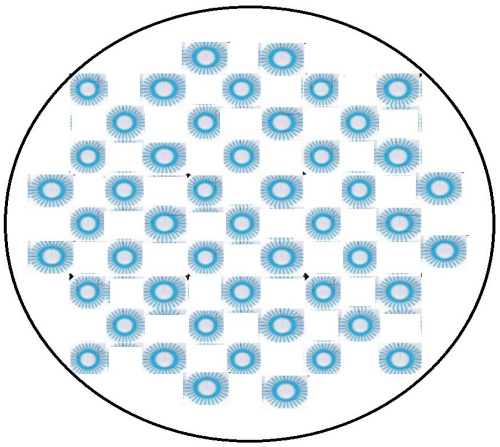

Figure 5. Thermosiphons with radially distributed axial fins for 49 heating pipes.

The tubes and fins are made of aluminum, and the thermal conductivity adopted is represented by the expression below.

$$k_W = 235\ \mathrm{W}/(\mathrm{m}\cdot\mathrm{K}) \tag{11}$$

The internal and external diameters of the thermosyphons are given by:

$$D_{int} = 50.08\ \mathrm{mm};\ D_{ext} = 50.973\ \mathrm{mm} \tag{12}$$

The length associated with the evaporator is given by:

$$L_{ev} = L'_{Ev}\text{, whith } \ L'_{Ev} \ \text{ function of filling rate EQ (03)} \tag{13}$$

The fin thickness and fin height are defined by the expressions below.

$$T_{Fin} = 4.0\ \mathrm{mm};\ \Delta H_{Fin} = 18.0\ \mathrm{mm} \tag{14}$$

The space between fins is obtained using the following expressions:

$$Sp_{Fin} = \left(P_{HP} - N_{Fin} * T_{Fin}\right)/\left(N_{Fin} + 1.0\right) \tag{15}$$

where,

$$P_{HP} = \pi D_{ext} \tag{16}$$

The shell diameter is expressed using the formula below.

$$D_{Shell} = 9.0 * \left(D_{ext} + 2 * \Delta H_{Fin}\right)\mathrm{mm} \tag{17}$$

The air intake area is expressed by:

$$A_{air} = \left(\pi D_{Shell}^2\right)/4 \tag{18}$$

The air passage area is obtained using the following expressions:

$$Asec_{air} = A_{air} - \left(NHP\left(\pi D_{ext}^2\right)/4\right) - \left(Ntot_{Fin} * \Delta H_{Fin} * T_{Fin}\right) \tag{19}$$

$$Asec_{air} = \left(\dot{m}_{air} Dh_{Ev}\right)/\left(Re_{air}\mu_{air}\right) \tag{20}$$

where,

$$Ntot_{Fin} = NHP * N_{Fin} \tag{21}$$

The hydraulic diameter in the evaporator is expressed by:

$$Dh_{Ev} = 4 * Asec_{air}/Ph_{Ev} \tag{22}$$

where,

$$Ph_{Ev} = NHP * P_{HP} + Ntot_{Fin} * \left(2 * \Delta H_{Fin} + T_{Fin}\right) \tag{23}$$

The heat exchange area between the fluids in the evaporator depends on two areas, namely:

$$A_{TotalEv} = Atr_{Fin} + Atr_{NHP} \tag{24}$$

where,

$$Atr_{Fin} = L_{Ev} * NHP * \left(2 * \Delta H_{Fin} + T_{Fin}\right) \tag{25}$$

The boiling coefficient is obtained through the Gupta and Varshney correlation [19].

$$h_{boil} = 1.39 * \left(k_{R404a} / l^*\right) * \left[Heat_{Flux} * \rho_{R404a} * Cp_{R404a} * l^* / \left(\rho_l * h_{lv} * k_{R404a}\right)\right]^{0.7} * \left(\rho_l / \rho_v\right)^{0.21} * \left(\mu_{R404a} * Cp_{R404a} / k^{R404a}\right)^{-0.21} \quad (26)$$

$Heat_{Flux}$ is determined from the Pioro correlation [20] [21]:

$$Heat_{Flux} = \mu_{R404a} * h_{lv} * l^* * \left[\left(1.0 / C_{sf}\right)^{0.33} * Pr_{R404a}^{1.0/0.33} * \left(Cp_{R404a} * \Delta T_{Evsat} / h_{lv}\right)^{1/0.33}\right] \quad (27)$$

where,

$$l^* = \left[\sigma_{R404a} / \left(g * \left(\rho_l - \rho_v\right)\right)\right]^{1/2} \quad (28)$$

The saturation temperature difference across the evaporator is represented by Equation (29).

$$\Delta T_{Evsat} = T_{airin} - T_{sat} \quad (29)$$

The Nusselt number associated with air is represented by equations below.

$$Nu_{airEv} = 0.696 * Re_{AirEv}^{0.5} * Pr_{air}^{0.36} * \left(Pr_{air} / \left(5.0 * Pr_{air}\right)\right)^{0.25} \quad (30)$$

where,

$$Re_{AirEv} = \left(4.0 * \dot{m}_{air}\right) / \left(\pi * Dh_{Ev} * \mu_{air}\right) \quad (31)$$

The heat transfer coefficient by air convection in the evaporator is obtained by:

$$h_{Ev} = Nu_{airEv} * k_{air} / D_{ext} \quad (32)$$

The application of the concept of "Aleta Analogy", conceived by Fakheri [22] leads us to define the following parameters:

$$mL_{EvFin} = \sqrt{\left(2h_{Ev}\right) / \left(k_{Fin} t_{Fin}\right)} * P_{hEv} \quad (33)$$

$$\eta_{EvFin} = \left(Tanh\left(mL_{EvFin}\right)\right) / \left(mL_{EvFin}\right) \quad (34)$$

The fin efficiency for the evaporator section is defined through Equation (34) by η_{EvFin} [15] [22]. This quantity is fundamental in theoretical and experimental studies on the thermal performance of fins and is widely used in finned systems analyzed by Élcio Nogueira [23].

$$\beta_{Ev} = A_{trFin} / A_{totEv} \quad (35)$$

$$\eta'_{EvFin} = \beta_{Ev} \eta_{EvFin} + \left(1 - \beta_{Ev}\right) \quad (36)$$

The global heat transfer coefficient associated with air in the Evaporator, Uo_{Ev}, is given by Equation (37).

$$Uo_{Ev} = 1 / \left(1 / h_{boil} + \left(D_{ext} - D_{int}\right) / k_W + 1 / \left(\eta'_{EvFin} h_{Evair}\right)\right) \quad (37)$$

The heat capacity of the air in the Evaporator is given by C_{Air}.

$$C_{Air} = \dot{m}_{air} Cp_{air} \quad (38)$$

The number of thermal units associated with air in the evaporator, NTU_{Ev}, is given by Equation (39).

$$NTU_{Ev} = \left(Uo_{Ev} * A_{totEv}\right) / C_{Ev}, \text{ where } C_{Ev} = C_{Air} \quad (39)$$

The dimensionless number, called "fin analogy", Fa_{Ev} is represented by Equation (40) as defined by Ahamad Fakheri [22] and reported by Nogueira, É. [15].

$$Fa_{Ev} = NTU_{Ev}/2 \text{ for parallel flow} \tag{40}$$

The thermal efficiency associated with the evaporator is η_{TEv} [14] [21].

$$\eta_{TEv} = \left(Tanh\left(Fa_{Ev}\right)\right)/\left(Fa_{Ev}\right) \tag{41}$$

$$\varepsilon_{TEv} = 1/\left(1/\left(\eta_{TEv} NTU_{Ev}\right)+1/2\right) \tag{42}$$

The thermal effectiveness associated with the heat evaporator is ε_{TEv}.

The heat transfer rate between the air and the heat pipe in the evaporating region $\dot{Q}_{Ev}$ is given by the Equation (43).

$$\dot{Q}_{Ev} = \left(C_{Ev}\Delta T_{Evsat}\right)/\left(1/\left(\eta_{TEv} NTU_{Ev}\right)+1/2\right) \tag{43}$$

After passing through the evaporator, the outlet air temperature is represented through Equation below.

$$T_{airout} = T_{airin} - \dot{Q}_{Ev}/C_{Ev} \tag{44}$$

After obtaining valid localized thermal quantities for the heat exchanger in steady state, a procedure is presented for determining average values for quantities of interest.

The equations below are associated with the average temperatures at the heat exchanger, along the axial direction in the evaporator region (Equations (45)-(49)).

The air temperature along the evaporator in the axial direction, as a function of the filling rate FR, is obtained by the expression represented by T'_{air}, Equation (46) below.

$$L'_{Ev} = FR * L_{Ev};\ \ 0.5 \le FR \le 1.0 \text{ ; defined in Equations (3)} \tag{45}$$

$$T'_{air} = \dot{Q}_{Ev}/\left(U'_{oEv} * A_{totEv} * \left(L_f/L'_{Ev}\right)\right) \tag{46}$$

T'_{air} is the temperature of the air in the axial direction. T'_{air} is dependent on the L_f position.

$$\Delta Hm \le L_f \le L'_{Ev};\ \ \Delta H = 10^{-4} \text{ by definition,} \tag{47}$$

$$U'_{oEv} = 1/\left(1/h_{boil} + \left(D_{ext} - D_{int}\right)/k_W\right) \tag{48}$$

where, U'_{oEv}, the global hate transfer coefficient, is associated with L'_{Ev}.

$$\dot{Q}_{Evf} = \dot{Q}_{Ev} - \dot{Q}_{Ev} * \left(\left(L_{Ev} - L_f\right)/L_{Ev}\right) \tag{49}$$

$\dot{Q}_{Evf}$ it is the rate of heat transfer, by definition, varying from the evaporator inlet to the position. L_f; $0 \le \dot{Q}_{Evf} \le \dot{Q}_{Ev}$.

When L_f is equal to L'_{Ev}, at the surface of the working fluid, the pressure equals P_{sat}.

$$T_W = T_f - \left(\dot{Q}_{Ev} * \left(\left(L'_{Ev} - L_f\right)/L'_{Ev}\right)\right)/C_{air} \text{ with } \Delta H \le L_f \le L'_{Ev} \tag{50}$$

T_W is the temperature on the wall of the heat pipe in the axial direction.

From the determination of the temperature profiles $T_f; T_W$ and $T'_{Tair}, \dot{Q}_{Evf}$,

the average temperatures, defined by $T_{fmed}; T_{Wmed}$ and T_{airmed}, are obtained through numerical integration.

The final expressions for $T_{fmed}; T_{Wmed}, T_{airoutmed}$ and $\dot{Q}_{Evmed}$ are described below:

$$T_{fmed} = \sum_{i=2}^{N-1} T_f + \left(\left(T_{f1} + T_{f2}\right)/2\right) * \left(L_f / L'_{Ev}\right) \text{ with } \Delta H \le L_f \le L'_{Ev} \quad (51)$$

$$T_{Wmed} = \sum_{i=2}^{N-1} T_W + \left(\left(T_{W1} + T_{W2}\right)/2\right) * \left(L_f / L'_{Ev}\right) \text{ with } \Delta H \le L_f \le L'_{Ev} \quad (52)$$

$$T_{airoutmed} = \sum_{i=2}^{N-1} T'_{air} + \left(\left(T'_{air1} + T'_{air2}\right)/2\right) * \left(L_f / L'_{Ev}\right) \text{ with } \Delta H \le L_f \le L'_{Ev} \quad (53)$$

$$\dot{Q}_{Evmed} = \sum_{i=2}^{N-1} \dot{Q}_{Evf} + \left(\left(\dot{Q}_{Evf1} + \dot{Q}_{Evf2}\right)/2\right) * \left(L_f / L'_{Ev}\right) \text{ with } \Delta H \le L_f \le L'_{Ev} \quad (54)$$

$T_{f1}, T_{W1}, T'_{air1}$ and $\dot{Q}_{Evf1}$ are obtained for $L_f = \Delta H$.
$T_{f2}, T_{W2}, T'_{air2}$ and $\dot{Q}_{Evf2}$ are obtained for $L_f = L'_{Ev}$.

2.3. First-Order Transient Analysis—Formulation for Evaporator

The system's base response time is obtained through the parameter τ, as a function of Equations (55)-(56) below.

$$\tau = h_{boil} * A_{totEv} / C_{Ev} \quad (55)$$

With C_{Ev} defined previously [Equation (39)].

$$t = \Delta t * \tau; \text{ with } 0 \le \Delta t \le 5 \text{ by definition} \quad (56)$$

$$T_{ft}(t) = T_{airin} + \left(T_{fmed} - T_{airin}\right) * \left(1 - e^{-\frac{t}{\tau}}\right) \quad (57)$$

$$T_{wt}(t) = T_{airin} + \left(T_{Wmed} - T_{airin}\right) * \left(1 - e^{-\frac{t}{\tau}}\right) \quad (58)$$

$$T_{airt}(t) = T_{airin} + \left(T_{airtmed} - T_{airin}\right) * \left(1 - e^{-\frac{t}{\tau}}\right) \quad (59)$$

$$\dot{Q}_{Ev}(t) = \dot{Q}_{Evmed} * \left(L_f / L'_{Ev}\right) * \left(1 - e^{-\frac{t}{\tau}}\right) \quad (60)$$

The T_{airin} air inlet temperature is selected as the reference because it is predetermined. The reference value for the heat exchange rate is equal to zero, since there is no heat exchange between the working fluid and the air temperature at the initial instant.

3. Results and Discussion

3.1. Steady State Regime

3.1.1. Local Results of the Physical Parameters of Interest as a Function of the Filling Rate

Figure 6 presents values for the heat exchange area as a function of the filling rate of the working fluid. For *FR* = 60%, the heat exchange area is 8 m², while the max-

imum value evaluated reaches approximately 14 m^2. These results will be important for the analysis that follows.

Figure 7 presents result for the local heat transfer rate exchanged between fluids as a function of the volume fraction of the working fluid. Higher air inlet temperatures increase heat exchange. The heat exchange rate between fluids is higher for lower filling fraction values and decreases significantly for higher values, although larger exchange area values are superior for higher filling fraction values.

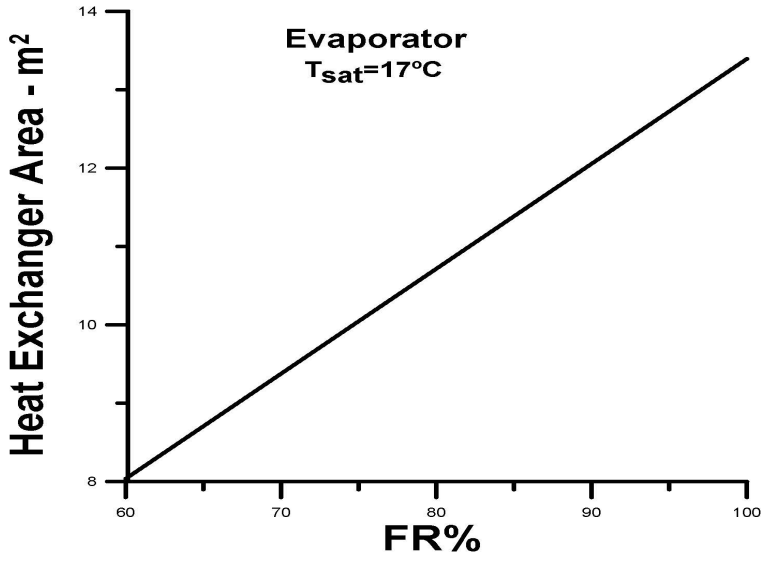

Figure 6. Heat exchange area versus working fluid filling rate.

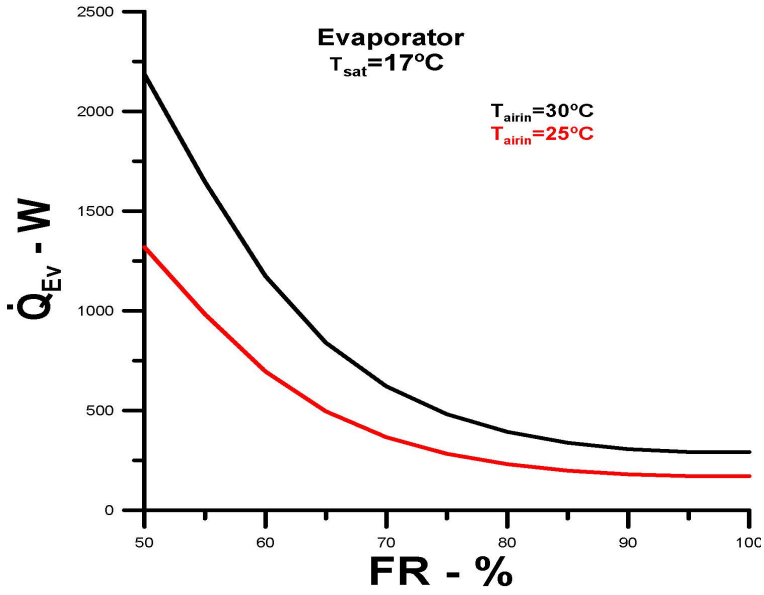

Figure 7. Heat transfer rate versus filling rate.

Figure 8 justifies the apparent contradiction regarding the heat exchange area, since the air outlet temperature, for small filling fraction values, tends towards the air inlet temperature, allowing for greater heat exchange between the air and the

working fluid. Conversely, as the filling ratio increases, the outlet temperature decreases, tending towards the fluid saturation temperature.

Figure 9 shows values for the wall temperature of the thermosiphons, along the radial direction and as a function of the filling rate of the working fluid. The surface temperature of the thermosiphons shows intermediate values between the working fluid temperature, Figure 4, and the air outlet temperature, Figure 8, tending towards the saturation temperature of the working fluid, when the possibility of heat exchange between the fluids decreases.

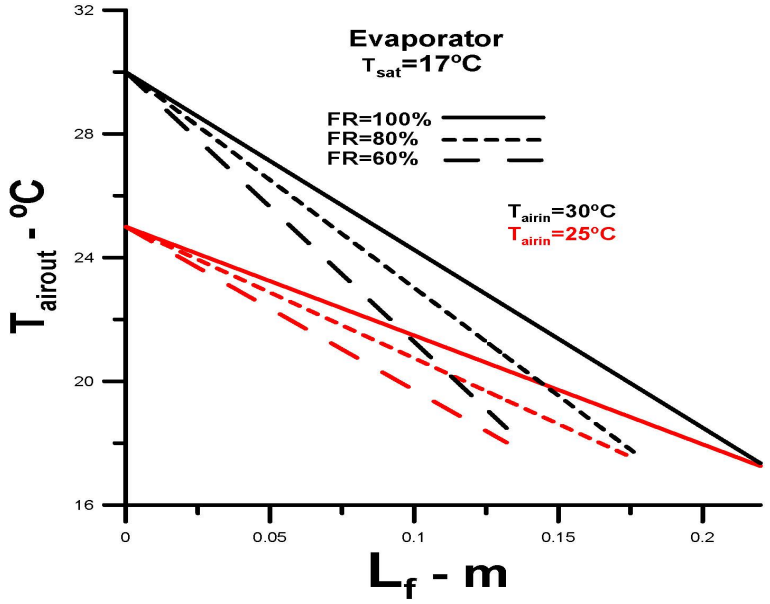

Figure 8. Air temperature profile along the axial direction as a function of the filling rate.

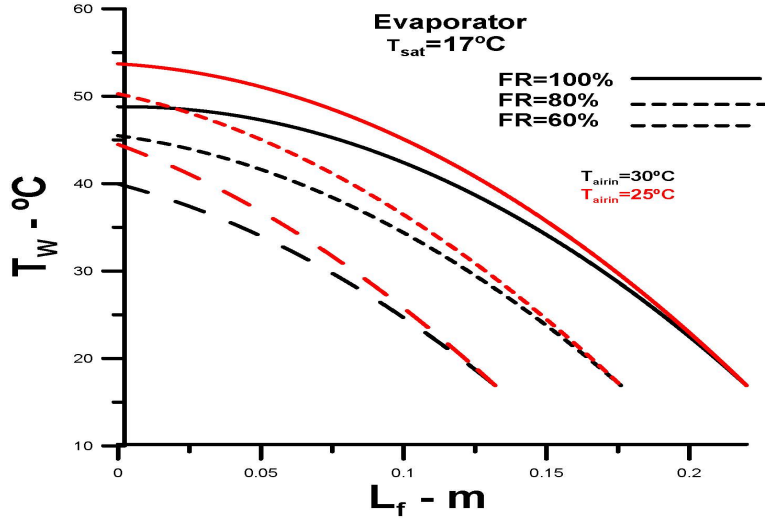

Figure 9. Temperature profile in the heat pipe wall as a function of the filling rate.

3.1.2. Average Values of Quantities of Interest as a Function of the Filling Rate

Figure 10 shows average temperature values for the working fluid, obtained from

the numerical integration of the working fluid temperature profiles presented in Figure 4. The values obtained by integration are very close to the values obtained through the arithmetic means, demonstrating the consistency of the procedure performed.

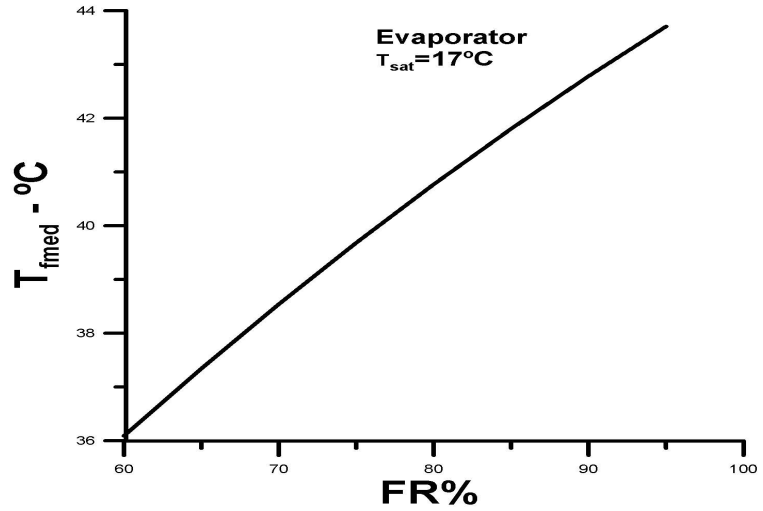

Figure 10. Average temperature profile of the working fluid as a function of the filling rate.

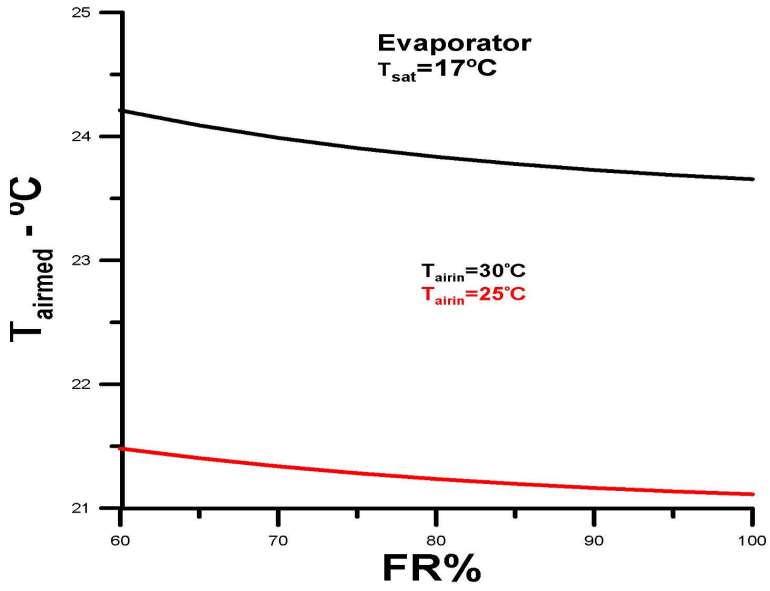

Figure 11. Average air temperature profile as a function of the filling rate.

Figure 11 presents average values for the mean air temperature as a function of the filling fraction of the working fluid and the air inlet temperatures. The temperature profiles used for the numerical determination of the average values are shown in Figure 8.

Figure 12 presents average values for the mean air temperature as a function of the filling fraction of the working fluid and the air inlet temperatures. The temperature profiles used for the numerical determination of the average values are

shown in Figure 9.

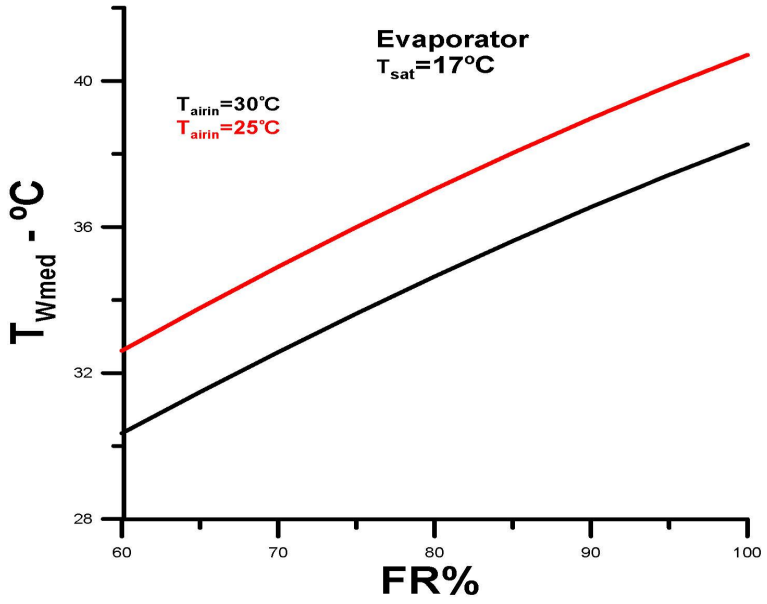

Figure 12. Average temperature profile of the heat pipe wall as a function of the filling rate.

3.2. First-Order Transient Regime

The simple first-order transient model assumes, in a first approach, the following hypotheses: lumped analysis, ripple-free time constant, negligible axial conduction, absence of dynamic occurrence between vapor and film, and negligible condensation.

The boundary and initial conditions are prescribed temperature on the thermosiphon wall, with air temperatures considered to be 25˚C and 30˚C. For the analysis of the variation in the heat transfer rate, an initial value of zero is imposed, since initially there is no heat exchange between the fluids.

The transient model adopted for the heat exchanger analysis in this work is feasible and appropriate, since the local values of the physical quantities of interest were determined and validated for steady-state conditions [13]. Furthermore, the heat exchanger under analysis exhibits perfect axial and radial homogeneity, allowing the equations applied for different filling rates to be used for a multi-thermosiphon bundle.

The main results obtained through the analysis carried out in this work are represented below. Figures 13-16 present results for transient regime, using average values of the physical quantities obtained and presented previously. The results obtained for average fluid temperatures, average tube wall temperatures, and air outlet temperatures use air inlet temperatures as references. Conversely, the reference temperature for the heat exchange rate is zero, since there is no heat exchange at the beginning of the process.

Figure 13 presents result for the average temperature of the working fluid as a function of the system response time. The parameters used in the analysis are the

filling rate of the working fluid and the air inlet temperatures (30˚C for solid line and 25˚C for dashed line). After 5 response times, as expected, the results converge to the established results for the previously determined average media values. Note that the system response times depend on the heat exchange area (EQ. 55) and, logically, depend on the filling rate of the working fluid.

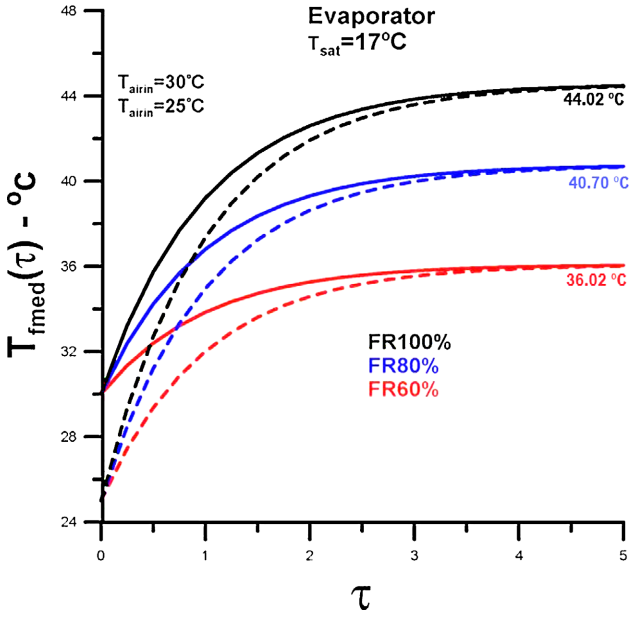

Figure 13. Response time of the average temperature of the work fluid.

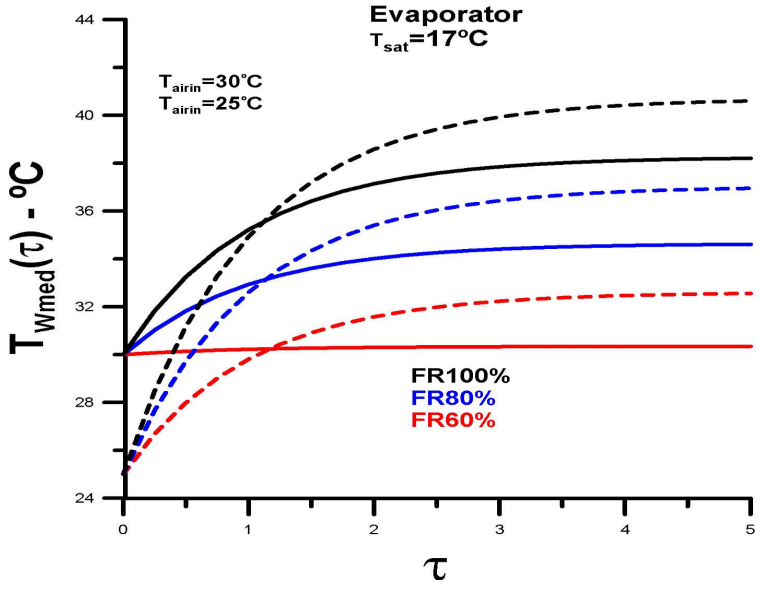

Figure 14. Response time of the average temperature on the wall of the heat pipe.

Figure 14 presents result for the average heat pipe wall temperature as a function of the system response time. The parameters used in the analysis are the filling rate of the working fluid and the air inlet temperatures (30˚ for the solid line and 25˚ for the dashed line). After 5 response times, as expected, the results con-

verge to the established average values previously determined. Note that the system response times depend on the heat exchange area (EQ. 55) and, logically, on the filling rate of the working fluid. A relevant fact to observe is that for a filling rate of 60% and an air inlet temperature of 30˚, the system presents a critical result, indicating that under these conditions the heat exchange has reached its operating limit. The result indicates that for higher inlet temperatures, the working fluid filling rate must be higher.

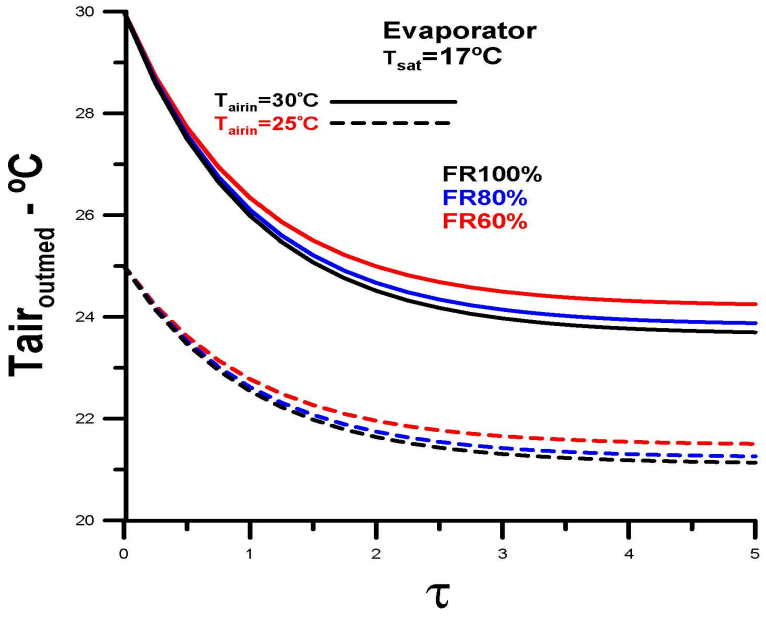

Figure 15. Response time of the average temperature of the air.

Figure 15 presents result for the average air outlet temperature in the evaporator as a function of the system response time. The parameters used in the analysis are the filling rate of the working fluid and the air inlet temperatures (30˚ for solid line and 25˚ for dashed line). After 5 response times, as expected, the results converge to the established results for the previously determined average values. Note that the system response times depend on the heat exchange area (EQ. 55) and, logically, depend on the filling rate of the working fluid.

Figure 16 presents result for the average heat exchange rate as a function of the system response time. The parameters used in the analysis are the filling rate of the working fluid and the air inlet temperatures (30˚ for solid line and 25˚ for dashed line). After 5 response times, as expected, the results converge to the established results for the previously determined average values. Note that the system response times depend on the heat exchange area (EQ. 55) and, logically, depend on the filling rate of the working fluid. It is observed that the heat exchange rates converge to higher values when subjected to higher inlet temperatures.

Figure 17 shows the values of τ and the total time for the system to reach steady state, using the inlet temperatures and the filling rate of the working fluid in the evaporator as parameters. The maximum response time, 719 seconds, corresponds

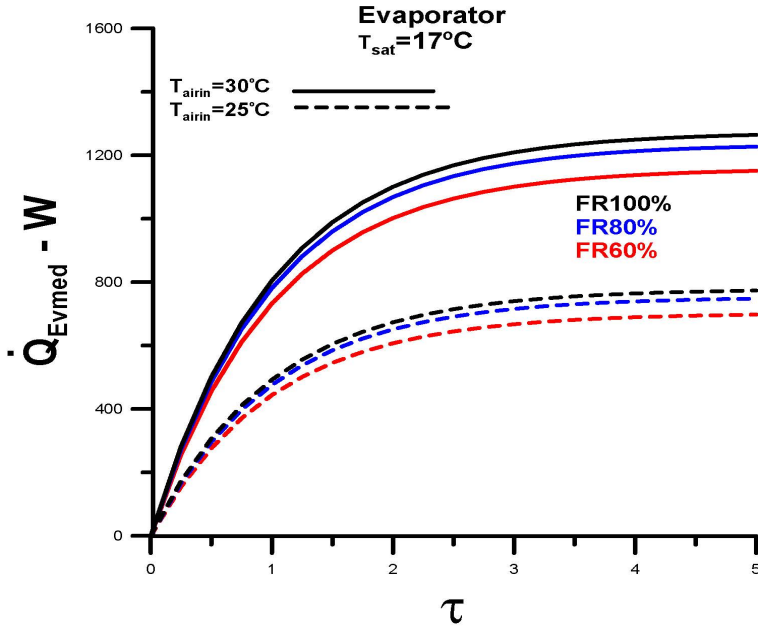

Figure 16. Response time of the average heat exchange rate.

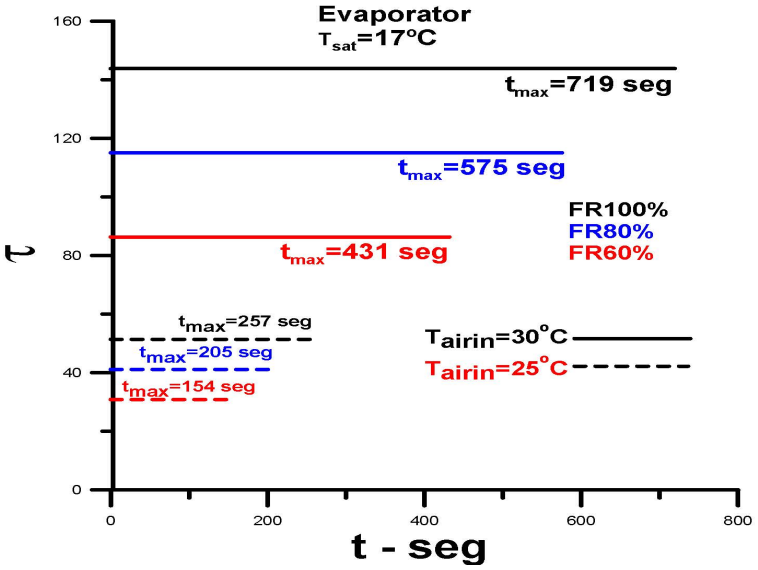

Figure 17. Response time for steady state versus filling rate.

to a temperature of 30˚C and FR = 100%. The minimum response time, 154 seconds, corresponds to a temperature of 25˚C and FR = 60%.

The time required for the system to reach steady state is summarized in Table 1 below.

Table 1. System response time for air temperature and fluid filling rate.

Air intake temperature	Working fluid filling rate	System response time
30˚C	100%	11.98 min
25˚C	100%	4.28 min

Continued

30˚C	80%	9.58 min
25˚C	80%	3.48 min
30˚C	60%	7.18 min
25˚C	60%	2.57 min

4. Conclusions

The objective of this work is to determine the transient response time of a heat exchanger with 49 finned thermosiphons.

To achieve the proposed objective, a well-established procedure was used to determine the average physical quantities of interest in steady state. The physical quantities analyzed are the heat transfer rate, the air outlet temperatures, the working fluid temperatures, and the thermosiphon wall temperatures.

The analysis involves varying the filling rate of the working fluid in the evaporator. The fluid used in the simulation is R404a, frequently used in refrigeration systems.

The variations in the filling rate used for analysis are 60%, 80%, and 100%. The system response time was determined for air inlet temperatures of 30˚C and 25˚C.

As expected, the first-order transient response determined for the system to reach steady state depends on the filling rate of the working fluid and the inlet air temperature in the heat exchanger. A higher filling rate, regardless of the inlet temperature, results in a longer time required to reach steady state. A higher air intake temperature, regardless of the filling rate, results in a longer time required for the system to reach steady state.

The conclusion obtained during the heat exchanger analysis is related to the filling rate of the working fluid: the limit on the filling rate, for an inlet air temperature of 30˚C, is 60%, because of the maximum wall temperature threshold (**Figure 14**).

Although the theoretical model appears logically consistent, its irrefutable validation depends on future experimental results, which represents a significant challenge.

Conflicts of Interest

The author declares no conflicts of interest regarding the publication of this paper.

References

[1] Farsi, H., Joly, J., Miscevic, M., Platel, V. and Mazet, N. (2003) An Experimental and Theoretical Investigation of the Transient Behavior of a Two-Phase Closed Thermosyphon. *Applied Thermal Engineering*, **23**, 1895-1912. https://doi.org/10.1016/s1359-4311(03)00147-9

[2] Storey, J.K. (2003) Modeling the Transient Response of a Thermosyphon. Ph.D. Thesis, Brigham Young University. https://scholarsarchive.byu.edu/etd/109

[3] Milanez, F.H. and Mantelli, M.B.H. (2006) Analytical Model for Thermal Perfor-

mance Analysis of an Enclosure Heated by Aligned Thermosyphons. *Journal of Thermophysics and Heat Transfer*, **20**, 267-275. https://doi.org/10.2514/1.14420

[4] Parand, R., Rashidian, B., Ataei, A. and Shakiby, K. (2009) Modeling the Transient Response of the Thermosyphon Heat Pipes. *Journal of Applied Sciences*, **9**, 1531-1537. https://doi.org/10.3923/jas.2009.1531.1537

[5] Amori, K.E. and Abdullah, M.L. (2013) Experimental and Theoretical Study of Two-Phase Heat Pipe. *Journal of Engineering*, **19**, 668-685.

[6] Jafari, D., Di Marco, P., Filippeschi, S. and Franco, A. (2017) An Experimental Investigation on the Evaporation and Condensation Heat Transfer of Two-Phase Closed Thermosyphons. *Experimental Thermal and Fluid Science*, **88**, 111-123. https://doi.org/10.1016/j.expthermflusci.2017.05.019

[7] Zhao, Z., Zhang, Y., Zhang, Y., Zhou, Y. and Hu, H. (2018) Numerical Study on the Transient Thermal Performance of a Two-Phase Closed Thermosyphon. *Energies*, **11**, Article 1433. https://doi.org/10.3390/en11061433

[8] Silveira, I. (2019) Theoretical and Experimental Study of Gravity-Assisted Heat Pipes for Applications in Solar Collectors. Ph.D. Thesis, University of Paraíba—Brazil. (In Portuguese)

[9] Nogueira, É. (2023) Thermal and Viscous Irreversibilities in the Heat Exchanger of Individually Finned Heat Pipes Using Freon R404A as the Working Fluid. *Mechanical Engineering Advances*, **1**, Article 132. https://doi.org/10.59400/mea.v1i1.132

[10] Liu, H., Wang, X., Zheng, L., Yao, H., Zhu, Y. and Wang, Y. (2022) Temperature Response and Thermal Performance Analysis of a Super-Long Flexible Thermosyphon for Shallow Geothermal Utilization: Field Test and Numerical Simulation. *International Journal of Heat and Mass Transfer*, **192**, Article ID: 122915. https://doi.org/10.1016/j.ijheatmasstransfer.2022.122915

[11] Brough, D.J. (2022) Transient Modelling of Heat Pipe Heat Exchangers with Vertical Thermosyphons for the Purpose of Waste Heat Recovery from Industrial Exhaust Gases. Ph.D. Thesis, Brunel University. https://bura.brunel.ac.uk/handle/2438/24580

[12] Zhang, W., Hao, W. and Wu, X. (2024) Development of Transient Thermal-Hydraulic Analysis Model for the Two-Phase Loop Thermosyphon. *Applied Thermal Engineering*, **243**, Article ID: 122764. https://doi.org/10.1016/j.applthermaleng.2024.122764

[13] Li, G., Zhang, Y., Zhang, G., Huang, S. and Ding, S. (2024) Transient Experimental and Numerical Study of Thermosyphon under Different Heating Fluxes and Filling Ratios. *Applied Thermal Engineering*, **243**, Article ID: 122514. https://doi.org/10.1016/j.applthermaleng.2024.122514

[14] Nogueira, É., Diniz, F.D.S.F., Felix, R. and Tavares, E.L.D.O. (2025) Evaluation of the Theoretical Design and Mathematical Modeling for Determination of Thermal and Viscous Irreversibilities in Axially Finned Two-Phase Closed Thermosyphon Heat Exchanger. *Journal of Materials Science and Chemical Engineering*, **13**, 48-78. https://doi.org/10.4236/msce.2025.1311005

[15] Nogueira, É. (2025) Heat Exchangers: Analytical Modeling and Applications. Editora Dialética. https://doi.org/10.48021/978-65-270-6139-7

[16] Bai, W., Geng, Z., Li, X., Wang, L., Shen, Y. and Chen, W. (2025) Transient Heat Transfer Characteristics and Flow Mechanism of Two-Phase Closed Thermosyphon. *International Communications in Heat and Mass Transfer*, **169**, Article ID: 109753. https://doi.org/10.1016/j.icheatmasstransfer.2025.109753

[17] Almeida, F.d.S., Brandalise, M.P., Rossi, R.R., Londoño Pabón, N.Y., Henriques Mantelli, M.B. and Mizgier, M.O. (2025) A Review of Heat Pipe and Thermosyphon Systems as Thermal Performance Strategies in Building Envelopes. *Energy and Buildings*, **329**, Article ID: 115310. https://doi.org/10.1016/j.enbuild.2025.115310

[18] Khalili, M., Mostafavi, S.A., Mousavi, S.M. and Moghadamrad, H. (2025) Optimizing Heat Transfer Performance in Two-Phase Closed Thermosyphons: A Novel Design and Experimental Evaluation. *Heliyon*, **11**, e42109. https://doi.org/10.1016/j.heliyon.2025.e42109

[19] Hameed, M.S., Khan, A.R. and Mahdi, A.A. (2013) Modeling a General Equation for Pool Boiling Heat Transfer. *Advances in Chemical Engineering and Science*, **3**, 294-303. https://doi.org/10.4236/aces.2013.34037

[20] Rohsenow, W.M. (1951) A Method of Correlating Heat Transfer Data for Surface Boiling of Liquids. Technical Report Nº 5, The Office Naval Research Contract N5ori-07827, Massachusetts Institute of Technology.

[21] Pioro, I.L., Rohsenow, W. and Doerffer, S.S. (2004) Nucleate Pool-Boiling Heat Transfer. II: Assessment of Prediction Methods. *International Journal of Heat and Mass Transfer*, **47**, 5045-5057. https://doi.org/10.1016/j.ijheatmasstransfer.2004.06.020

[22] Fakheri, A. (2006) Heat Exchanger Efficiency. *Journal of Heat Transfer*, **129**, 1268-1276. https://doi.org/10.1115/1.2739620

[23] Nogueira, E. (2020) Analytical and Numerical Methods with Engineering Applications in Heat Transmission and Fluid Mechanics. Editora Appris, 201 p.

Nomenclature

$Asec$	cross-section area, [m^2]
Atr	heat transfer area, [m^2]
Cp	specific heat, J/(kgK)
C	thermal capacity, [W/K]
C_{min}	minimum thermal capacity, [W/K]
D_h	hydraulic diameter, [m]
Fa	fin analogy
h	coefficient of heat convection, [W/(m^2 K)]
k	thermal conductivity, [W/mK]
K	Kelvin
k_W	thermal conductivity of the tube, [W/mK]
k_{Fin}	thermal conductivity of the fin, [W/mK]
L	vertical or horizontal length, [m]
$\dot{m}_{air}$	mass flow rate of the air, [kg/s]
N_{Fin}	number of fins
Nu	Nusselt number
Pr	Prandtl number
$\dot{Q}$	actual heat transfer rate, [W]
$\dot{Q}_{max}$	maximum heat transfer rate, [W]
Re	Reynolds number
T	temperatures, [˚C]
Uo	global heat transfer coefficient, [W/(m^2 K)]

Subscripts

boil	ebulição
Cd	Condenser
Cond	Condenser
effect	effective
Ev	Evaporator
ext	external

HP	heat pipe
H	horizontal
in	inlet
int	internal
out	outlet
sat	saturation

Greek Symbols

α	thermal diffusivity, [m^2/s]
β	the relationship between areas
ρ	density of the fluid, [kg/m^3]
μ	dynamic viscosity of fluid, [kg/ms]
ν	kinematic viscosity of the cold fluid, [m^2/s]
ε_T	thermal effectiveness
η_T	thermal efficiency
ΔT	a difference of temperatures, [˚C]

Acronyms

FHPHE	Finned heat pipe heat exchanger
Ev	Evaporators
Cd	Condenser
NHP	Number of Heat Pipes
NFin	Number of Fins
Nrows	Number of rows
NTU	Number of thermal units